IEEE Access
Multidisciplinary | Rapid Review | Open Access Journal

Received March 26, 2021, accepted April 16, 2021, date of publication April 27, 2021, date of current version June 15, 2021.

Digital Object Identifier 10.1109/ACCESS.2021.3076001

A New Method for Predicting the Crack Propagation Process of Brittle Rock Under Thermo-Hydro-Mechanical Loading Conditions

WEI YI[1], QIUHUA RAO[1], ZHUO LI[1], AND CHARLIE CHUN-LIN LI[2]
[1]School of Civil Engineering, Central South University, Changsha 410075, China
[2]Department of Geoscience and Petroleum, The Norwegina University of Science and Technology, Trondheim 7491, Norway

Corresponding author: Qiuhua Rao (raoqh@csu.edu.cn)

This work was supported in part by the National Natural Science Foundation of China under Grant 51474251and Grant 51874351, and in part by the Excellent Postdoctoral Innovative Talents Project of Hunan Province under Grant 2020RC2001.

ABSTRACT Prediction on the crack propagation process of brittle rock under Thermo-Hydro-Mechanical (THM) loading conditions is very important for crack-arrest design and disaster prevention in deep rock engineering. Although currently existing fracture criteria can successfully predict crack initiation under arbitrary loading conditions, very few quantitative methods are available for predicting the crack propagation process of brittle rock under single loading condition, let alone THM loading conditions. In this paper, a new THM coupling fracture theory is established to predict the crack propagation process (including the crack initiation, stable and unstable propagation of Mode I or Mode II fracture), where the calculation formulae of Mode I and Mode II wing-tip stress intensity factors are deduced by a new superposition method with higher accuracy than the conventional superposition method and simpler form than the complex function method. Uniaxial compression tests and self-designed THM coupling tests of pre-cracked specimens are conducted to measure stress-strain curves and fracture trajectories under different loading conditions. Research results show that mechanism of crack initiation is the same as that of unstable propagation in both uniaxial compression and THM coupling tests. As the temperature and hydraulic pressure are increased and the confining pressure is decreased, the mechanisms of crack initiation and unstable propagation are changed from Mode II to Mode I. Mode I fracture has smaller loads of crack initiation load and unstable propagation and larger length of crack stable propagation than Mode II fracture. Test results agree very well with prediction ones, which proves the validity of the new THM coupling fracture theory. This fracture theory can be further extended to predict the multi-crack propagation process under THM loading conditions.

INDEX TERMS Crack propagation process, THM coupling fracture theory, wing-tip stress intensity factors, THM cupling test, brittle rock.

NOMENCLATURE

a, c, φ, E	crack half-length, cohesion, internal friction angle and Young's modulus
$K_{IC}^{ini,T}$, $K_{IIC}^{ini,T}$	initial cracking toughness of Mode I and Mode II related to temperature
$K_{IC}^{un,T}$, $K_{IIC}^{un,T}$	unstable fracture toughness of Mode I and Mode II related to temperature
$K_I^{HM}(\theta)$, $K_{II}^{HM}(\theta)$	Mode I and Mode II stress intensity factors on the original crack plane
$K_I^{HM}(i)$, $K_{II}^{HM}(i)$	$i = \alpha, \beta$; Mode I and Mode II stress intensity factors at an arbitrary angle of i
$K_I^{HM}(i)_{\max}$, $K_{II}^{HM}(i)_{\max}$	$i = \alpha, \beta$; maximum Mode I and Mode II stress intensity factors at an arbitrary angle of i
$K_I^{2a,HM}(\alpha)$, $K_{II}^{2a,HM}(\alpha)$	additional Mode I and Mode II stress intensity factor
$K_I^{l,HM}(\alpha)$, $K_{II}^{l,HM}(\alpha)$	Mode I and Mode II stress intensity factor of the isolated wing crack plane

The associate editor coordinating the review of this manuscript and approving it for publication was Wenming Cao.

$K_I^{w,HM}(\alpha)$, $K_{II}^{w,HM}(\alpha)$	Mode I and Mode II stress intensity factors on the wing crack plane
L, l_C	wing crack length, subcritical extension length
l_{eq}	half length of the equivalent crack
l_{IC}, l_{IIC}	subcritical extension length of Mode I and Mode II
P, P_C^{ini}, P_C^{un}	axial pressure, crack initiation load and unstable propagation load
P_{IC}^{ini}, P_{IIC}^{un}	crack initiation load of Mode I and Mode II under THM loading conditions
P_{IC}^{un}, P_{IIC}^{un}	unstable propagation load of Mode I and Mode II under THM loads
P_{LIC}^{ini}, P_{LIIC}^{un}	initial cracking load of Mode I and Mode II in three-point bending and shear-box tests
P_{LIC}^{un}, P_{LIIC}^{un}	unstable fracture load of Mode I and Mode II in three-point bending and shear-box tests
P_x, Q_x	symmetrical concentrated normal and shear force on the crack plane
r_1, α *and* r_2, β	two conventional polar coordinate
T, P_H, P_M	temperature, hydraulic pressure and confining pressure
α_C, β_C	crack initiation angle, unstable initiation angle
α_{IC}, α_{IIC}	crack initiation angle of Mode I and Mode II
β_{IC}, β_{IIC}	unstable initiation angle of Mode I and Mode II
θ, μ	inclination of the original crack, friction coefficient
σ_c, σ_t	uniaxial compressive strength, tensile strength
τ_{eff}	effective shear stress on the original crack plane
σ_{eq}, τ_{eq}	equivalent normal and shear stress on the equivalent crack plane
σ_n, τ_n	normal and shear stress on the original crack plane
σ_α, $\tau_{r\alpha}$	stress components at the original crack tip

I. INTRODUCTION

In deep rock engineering, such as oil and natural gas exploitation, geothermal development, underground energy storage, rock mass is usually subjected to thermo-hydro-mechanical (THM) coupled loading conditions [1]–[4]. Pre-existing geological discontinuities or joints in the rock mass may be extended or new fractures are initiated under such coupled loading conditions. How to predict the crack propagation process (including crack initiation, stable and unstable propagation) of brittle rock becomes a hot issue since it is very important for safety assessment, crack-arrest design and disaster prevention in rock engineering [5]–[7].

Recently, there are mainly two types of methods for studying fracture trajectory: experimental method and theoretical method. Extensive experimental studies were performed on crack initiation and propagation in pre-cracked specimens of brittle materials (including molded gypsum [8], [9], glass [10], rock [11]–[15] and concrete [16]–[18]) under un-axial and bi-axial compressions, and multi-field loading conditions. In general, when specimen with a single crack is subjected to uniaxial compression, the original crack is initiated and propagated from its two crack-tips along the direction of axial stress, with Mode I (tensile) failure [8]–[11], [14], [15], [18]. Under biaxial or conventional triaxial compression loads with a high confining pressure, the specimens usually produce mode II (shear) failure [16]. However, it is very difficult to exactly determine the stress state within specimen and predict crack propagation path under different loading conditions. Therefore, theoretical method draws more and more attention of many researchers. Fracture criterion is the key to predicting the crack initiation and current fracture criteria can be divided into three categories: 1) stress-based fracture criterion, such as maximum tensile stress criteria (σ_θ-criterion) [19], maximum tangential principle stress criterion ($\sigma_{1\theta}$-criterion) [20] and twin shear stress criterion [21], 2) strain-based fracture criteria, such as maximum tangential strain criterion (ε_θ-criterion) [22], and 3) energy-based fracture criteria, such as minimum strain energy density criterion (S-criterion) [23], maximum energy release rate criterion (G-criterion) [24], [25], maximum volumetric strain energy density criterion (T-criterion) [26]–[28], and maximum distortional strain energy release rate criterion (Y-criterion) [29]. These criteria can successfully predict crack initiation of most materials (e.g., metal and glass) under pure tensile [20]–[32] and shear [33]–[36], and mixed loading conditions [37]–[43]. For brittle rock, pure shear loading applied on a pre-existing crack is not certain to lead to Mode II fracture, and Mode I fracture is easy to occur before Mode II fracture is initiated under pure shear loading condition [44], [45], since the tensile strength of rock is substantially smaller than its shear strength. Compressive load has to be applied onto the original crack plane (i.e., under compression-shear loading) in order to restrain the tensile stress at crack tip for facilitating occurrence of Mode II fracture. Thus, a new mixed mode fracture criterion was proposed based on ratio of the maximum tensile and shear stress intensity factors [44]. It can successfully predict Mode I or Mode II crack initiation under mixed mode loading conditions [44]–[47] as well as THM loading fields [48]. It could be used to predict the crack propagation process by considering the wing-tip stress intensity factor after crack initiation. On the other hand, although some fracture criteria were extended to study effect of temperature and hydraulic pressure on crack initiation [49]–[54], very few literature is related to establish a systematical quantitative method for predicting the crack propagation process (including the crack initiation, stable and unstable propagation) of rock under THM loading conditions.

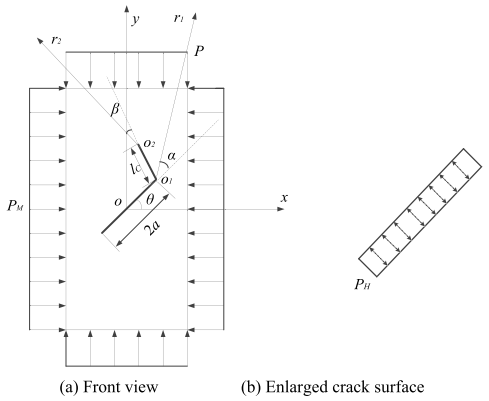

FIGURE 1. Calculation model of a pre-cracked rock specimen under THM loading conditions.

In the paper, a new THM coupling fracture theory is established to predict the crack propagation process (including the crack initiation, stable and unstable propagation) of brittle rock under THM loading conditions. The calculation formula for Mode I and Mode II wing-tip stress intensity factor are deduced through a new superposition method. Uniaxial compression and self-designed THM coupling tests are conducted on pre-cracked specimens under different loading conditions to obtain stress-strain curves and fracture trajectories and to verify the validity of the new established THM coupling fracture theory.

II. THM COUPLING FRACTURE THEORY

A. CALCULATION MODEL

Fig.1 depicts a cylindrical rock specimen (Φ50mm × 100mm) of an oriented penetrating crack ($2a$ = 30mm and θ = 45°) under THM loading conditions (i.e., temperature T, hydraulic pressure P_H, confining pressure P_M and axial pressure P, where tensile stress is defined as positive). A global rectangular coordinate system (xoy) is set at the center of the crack surface (o), and two polar coordinate systems (o_1r_1 and o_2r_2) are set at the crack tip (o_1) and the wing crack tip (o_2), respectively. As the axial load is increased, the crack would initiate at an angle of α (crack initiation angle), and then extend for a length of l_C (stable propagation length, approximately in straight line) and finally unstably propagate at an angle of β (unstable initiation angle), where counter-clockwise angle is defined as positive.

Table 1 lists different THM loading conditions for the pre-cracked rock specimens. Considering the actual temperature in deep rock engineering (usually at least 1000m in depth) is about 50°C in most region (temperature gradient of 0.016°C/m∼0.027°C/m) [55], the testing temperatures are selected to be 25°C, 50°C, 70°C, 90°C (smaller than 100°C for preventing water from evaporation). Although the actual confining pressures in deep rock engineering is about 18MPa∼38MPa, the testing confining pressures are selected to be 2.5MPa, 3MPa, 4MPa, 4.5MPa. That is because when P_M > 6MPa, the isolation films wrapped on the pre-cracked specimen would be penetrated and the confining pressure fails to be applied. P_H must be smaller than P_M for avoiding the mixture of water (applying hydraulic pressure) and oil (applying confining pressure), and P_H are selected to be 0.5MPa, 1.5MPa, 2MPa, 3.5MPa.

TABLE 1. Pre-cracked rock specimens under different THM loading conditions.

Specimen No.	T (℃)	P_H (MPa)	P_M (MPa)
T1	25	2	4
T2	50	2	4
T3	70	2	4
T4	90	2	4
H1	70	0.5	4
H2	70	1.5	4
H3	70	3.5	4
M1	50	2	2.5
M2	50	2	3
M3	50	2	4.5

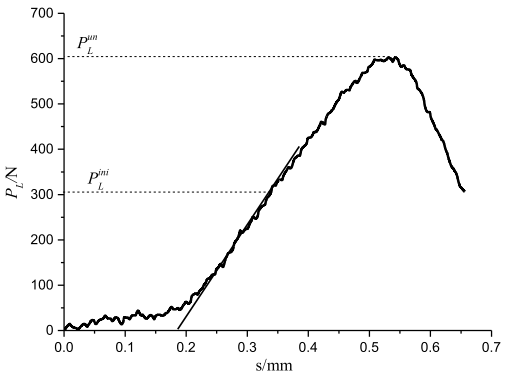

FIGURE 2. Load-displacement curve of the rock specimen in three-point bending test (T = 25°C).

Table 2 lists the initial cracking toughness and unstable fracture toughness of rock specimens under different THM loading conditions. Since the rock fracture toughness is a material parameter related to temperature, three-point bending tests and shear-box tests of the rock specimens at different temperatures (T = 25°C, 50°C, 70°C, 90°C) were performed to determine the initial cracking load of Mode I and Mode II (P_{LIC}^{ini} and P_{LIIC}^{ini}, at the distinguished point of straight and curved lines) and unstable fracture load of Mode I and Mode II (P_{LIC}^{un} and P_{LIIC}^{un}, at the peak point) by its load-displacement curves (e.g., Fig. 2), respectively. The initial cracking toughness of Mode I and Mode II (K_{IC}^{ini} and K_{IIC}^{ini}), and unstable fracture toughness of Mode I and Mode II (K_{IC}^{un} and K_{IIC}^{un}) can be calculated, as tabulated in Table 2.

TABLE 2. Initial cracking toughness and unstable fracture toughness of rock specimens under different temperatures (MPa · $m^{0.5}$).

T(℃)	$K_{IC}^{ini,T}$	$K_{IIC}^{ini,T}$	$K_{IC}^{un,T}$	$K_{IIC}^{un,T}$
25	0.60	1.31	1.21	2.11
50	0.55	1.25	1.13	2.07
70	0.48	1.22	1.04	2.01
90	0.41	1.19	0.89	1.96

B. FRACTURE CRITERION

1) CRACK INITIATION CRITERION

Under THM loading conditions, the normal stress (σ_n) and shear stress (τ_n) on the original crack plane can be express as

$$\begin{aligned}\sigma_n &= \frac{(P+P_M)}{2} + \frac{(P-P_M)}{2}\cos 2\theta + P_H \\ \tau_n &= \frac{(P-P_M)}{2}\sin 2\theta\end{aligned} \tag{1}$$

Considering the effect of σ_n on τ_n, the effective shear stress τ_{eff} is can be given by

$$\tau_{eff} = \tau_n + \mu\,|\sigma_n| \tag{2}$$

where μ is the Coulomb friction coefficient. When $\mu = 0$, the original crack is open after the crack initiation.

Thus, Mode I and Mode II stress intensity factors on the original crack plane can be expressed as

$$\begin{aligned}K_I^{HM}(\theta) &= \sigma_n\sqrt{\pi a} \\ &= [\frac{(P+P_M)}{2} + \frac{(P-P_M)}{2}\cos 2\theta + P_H]\sqrt{\pi a} \\ K_{II}^{HM}(\theta) &= \tau_{eff}\sqrt{\pi a} = \frac{(P-P_M)}{2}\sin 2\theta\sqrt{\pi a} \\ &\quad + \mu\sqrt{\pi a}\left|\frac{(P+P_M)}{2} + \frac{(P-P_M)}{2}\cos 2\theta + P_H\right|\end{aligned} \tag{3}$$

When the original crack is initiated at an arbitrary angle of α ($\alpha > 0$ or $\alpha < 0$, Fig. 3), stress components at the crack tip become

$$\begin{aligned}\sigma_\alpha &= \frac{K_I^{HM}(\theta)}{\sqrt{2\pi r}}\cos^3\frac{\alpha}{2} - \frac{3K_{II}^{HM}(\theta)}{\sqrt{2\pi r}}\sin\frac{\alpha}{2}\cos^2\frac{\alpha}{2} \\ \tau_{r\alpha} &= \frac{K_I^{HM}(\theta)}{\sqrt{2\pi r}}\sin\frac{\alpha}{2}\cos^2\frac{\alpha}{2} + \frac{K_{II}^{HM}(\theta)}{\sqrt{2\pi r}}\cos\frac{\alpha}{2}(1-3\sin^2\frac{\alpha}{2})\end{aligned} \tag{4}$$

Substituting Eq. (4) into the definition of the Mode I and Mode II stress intensity factors at an arbitrary angle of α :

$$\begin{aligned}K_I^{HM}(\alpha) &= \lim_{r\to 0}(\sigma_\alpha\sqrt{2\pi r}) \\ K_{II}^{HM}(\alpha) &= \lim_{r\to 0}(\tau_{r\alpha}\sqrt{2\pi r})\end{aligned} \tag{5}$$

results in:

$$K_I^{HM}(\alpha) = K_I^{HM}(\theta)\cos^3\frac{\alpha}{2} - 3K_{II}^{HM}(\theta)\sin\frac{\alpha}{2}\cos^2\frac{\alpha}{2}$$

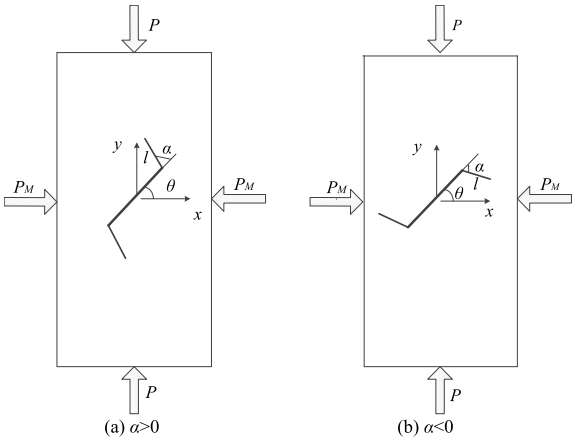

FIGURE 3. Crack initiation under THM loading conditions.

$$\begin{aligned}K_{II}^{HM}(\alpha) &= K_I^{HM}(\theta)\sin\frac{\alpha}{2}\cos^2\frac{\alpha}{2} \\ &\quad + K_{II}^{HM}(\theta)\cos\frac{\alpha}{2}(1-3\sin^2\frac{\alpha}{2})\end{aligned} \tag{6}$$

From the viewpoints of common fracture criteria, the fracture mode (Mode I or Mode II fracture) is consistent with the loading mode (tensile or shear), which is suitable for most metallic materials. However, for brittle rock and rock-like materials, their tensile strength is much smaller than shear strength, and pure shear loading usually results in tensile (Mode I) fracture rather than shear (Mode II) fracture. The fracture mode depends on the maximum stress intensity factor ratio of the crack tip, i.e. the stress field rather than the loading mode. And thus, a new criterion of maximum tensile and shear stress intensity factor ratio was established in our previous work [44]. Based on the new fracture criterion, crack initiation criterion can be obtained as follows:

$$\begin{cases}\dfrac{K_{II}^{HM}(\alpha)_{\max}}{K_I^{HM}(\alpha)_{\max}} < \dfrac{K_{IIC}^{ini,T}}{K_{IC}^{ini,T}} \\ K_I^{HM}(\alpha)_{\max} = K_{IC}^{ini,T}\end{cases} \text{Crack initiation in Mode I}$$

or

$$\begin{cases}\dfrac{K_{II}^{HM}(\alpha)_{\max}}{K_I^{HM}(\alpha)_{\max}} > \dfrac{K_{IIC}^{ini,T}}{K_{IC}^{ini,T}} \\ K_{II}^{HM}(\alpha)_{\max} = K_{IIC}^{ini,T}\end{cases} \text{Crack initiation in Mode II} \tag{7}$$

Accordingly, the crack initiation angle (α_{IC} and α_{IIC}) and load (P_{IC}^{ini} and P_{IIC}^{ini}) in Mode I and Mode II can be calculated:

$$\begin{cases}\dfrac{\partial K_I^{HM}(\alpha)}{\partial\alpha} = 0, \quad \dfrac{\partial^2 K_I^{HM}(\alpha)}{\partial\alpha^2} < 0 \\ K_I(\alpha)_{\max} = K_{IC}^{ini,T}\end{cases}$$

$$\Rightarrow \begin{cases}\alpha_{\text{IC}} & \text{Crack initiation} \\ P_{IC}^{ini} & \text{in Mode I}\end{cases}$$

or

$$\begin{cases}\dfrac{\partial K_{II}^{HM}(\alpha)}{\partial\alpha} = 0, \quad \dfrac{\partial^2 K_{II}^{HM}(\alpha)}{\partial\alpha^2} < 0 \\ K_{II}^{HM}(\alpha)_{\max} = K_{IIC}^{ini,T}\end{cases}$$

$$\Rightarrow \begin{cases} \alpha_{\mathrm{IIC}} & \text{Crack initiation} \\ P_{IIC}^{ini} & \text{in Mode II} \end{cases} \tag{8}$$

Whether the crack initiates in Mode I at α_{IC} or in Mode II at α_{IIC} depends on whether the crack initiation load P_{IC}^{ini} or P_{IIC}^{ini} is smaller, i.e.,

$$P_{IC}^{ini} < P_{IIC}^{ini} \Rightarrow \begin{cases} P_C = P_{IC}^{ini} \\ \alpha_C = \alpha_{IC} \end{cases} \quad \text{Crack initiation in Mode I}$$
$$\text{or}$$
$$P_{IC}^{ini} > P_{IIC}^{ini} \Rightarrow \begin{cases} P_C = P_{IIC}^{ini} \\ \alpha_C = \alpha_{IIC} \end{cases} \quad \text{Crack initiation in Mode II} \tag{9}$$

2) CRACK STABLE AND UNSTABLE PROPAGATION CRITERION

As shown in Fig.1, when the crack initiation criterion (Eq. 7) is satisfied, the original crack is initiated at an angle of α_{IC} (in Mode I) or α_{IIC}(in Mode II), then extended for a length of l_{Ic} or l_{IIc} (stable propagation length, approximately in straight line) and finally unstably propagated at an angle of β_{IC} (in Mode I) or β_{IIC} (in Mode II) when Mode I stress intensity factor on the wing crack plane α ($K_I^{w,HM}(\alpha)$) reaches $K_{IC}^{ini,T}$ or Mode II stress intensity factor on the wing crack plane α ($K_{II}^{w,HM}(\alpha)$) reaches $K_{IIC}^{ini,T}$. A new crack unstable propagation criterion can be established based on criterion of maximum tensile and shear stress intensity factor ratio as follows.

$$\begin{cases} K_I^{w,HM}(\alpha)_{\max} = K_{IC}^{ini,T} \\ \dfrac{\partial K_I^{HM}(\beta)}{\partial \beta} = 0, \quad \dfrac{\partial^2 K_I^{HM}(\beta)}{\partial \beta^2} < 0 \\ K_I^{HM}(\beta)_{\max} = K_{IC}^{un,T} \end{cases}$$
$$\Rightarrow \begin{cases} l_{IC} \\ \beta_{\mathrm{IC}} \\ \mathrm{P}_{IC}^{un} \end{cases} \quad \text{Crack unstable propagation in Mode I}$$
$$\text{or}$$
$$\begin{cases} K_I^{w,HM}(\alpha)_{\max} = K_{IIC}^{ini,T} \\ \dfrac{\partial K_{II}^{HM}(\beta)}{\partial \beta} = 0, \quad \dfrac{\partial^2 K_{II}^{HM}(\beta)}{\partial \beta^2} < 0 \\ K_{II}^{HM}(\beta)_{\max} = K_{IIC}^{un,T} \end{cases}$$
$$\Rightarrow \begin{cases} l_{IIC} \\ \beta_{\mathrm{IIC}} \\ \mathrm{P}_{IIC}^{un} \end{cases} \quad \text{Crack unstable propagation in Mode II} \tag{10}$$

where $K_{IC}^{un,T}$ and $K_{IIC}^{un,T}$ are unstable fracture toughness of Mode I and Mode II related to the temperature (Table 2), respectively; $K_I^{HM}(\beta)$ and $K_{II}^{HM}(\beta)$ are Mode I and Mode II stress intensity factor of the wing crack at an arbitrary angle (β), which can be obtained from the next section.

Similar to Eq. (6), one obtains

$$K_I^{HM}(\beta) = K_I^{w,HM}(\alpha)\cos^3\frac{\beta}{2} - 3K_{II}^{w,HM}(\alpha)\sin\frac{\beta}{2}\cos^2\frac{\beta}{2}$$
$$K_{II}^{HM}(\beta) = K_I^{w,HM}(\alpha)\sin\frac{\beta}{2}\cos^2\frac{\beta}{2} + K_{II}^{w,HM}(\alpha)\cos\frac{\beta}{2}(1-3\sin^2\frac{\beta}{2}) \tag{11}$$

Whether the crack unstable propagation in Mode I at β_{IC} or in Mode II at β_{IIC} depends on whether the unstable propagation load P_{IC}^{un} or P_{IIC}^{un} is smaller, i.e.,

$$P_{IC}^{un} < P_{IIC}^{un} \Rightarrow \begin{cases} P_C = P_{IC}^{un} \\ \beta_C = \beta_{IC} \end{cases} \quad \begin{matrix} \text{Crack unstable propagation} \\ \text{in Mode I} \end{matrix}$$
$$\text{or}$$
$$P_{IC}^{un} > P_{IIC}^{un} \Rightarrow \begin{cases} P_C = P_{IIC}^{un} \\ \beta_C = \beta_{IIC} \end{cases} \quad \begin{matrix} \text{Crack unstable propagation} \\ \text{in Mode II} \end{matrix} \tag{12}$$

It should be noted here that the effect of temperature is considered by the fracture toughness at different temperature. This is because all of rock specimens have the same temperature in this study and thus no thermal stress affects the normal and shear stresses directly in the new established theory.

In addition, Some well-known mixed mode fracture models, such as. ASED, GMTS, GMTSN (EMTSN), TSC, MTSN, MSED, are usually used to predict the Mode I crack initiation under arbitrary loading conditions (tension, shear and tension-shear mixed load) but less to predict both the Mode II crack initiation and the whole propagation process of brittle rock. The new fracture theory established based on our fracture criterion of maximum tensile and shear SIF ratio [43] can not only predict the crack initiation of both Mode I and Mode II, but also predict the whole process of crack stable and unstable propagation for better understanding the fracture mechanism of brittle rock under thermo-hydro-mechanical loading conditions. Although only single-crack problem is considered in the above analysis, the newly established fracture theory can also be extended to study multi-crack problem by obtaining the interacting stress intensity factors [56].

C. STRESS INTENSITY FACTOR FORMULA OF WING CRACK

For predicting crack stable propagation under THM loading conditions, it is necessary to deduce Mode I and Mode II stress intensity factor formulae of the wing crack initiated by tension ($\alpha > 0$) or shear ($\alpha < 0$) of the original crack as follows

1) WING CRACK INITIATED BY TENSION ($\alpha > 0$)

As shown in Fig. 4, Mode I and Mode II stress intensity factors on the wing crack plane (α) can be obtained by the superposition method [57]:

$$K_I^{w,HM}(\alpha) = K_I^{l,HM}(\alpha) + K_I^{2a,HM}(\alpha)$$
$$K_{II}^{w,HM}(\alpha) = K_{II}^{l,HM}(\alpha) + K_{II}^{2a,HM}(\alpha) \tag{13}$$

where $K_I^{l,HM}(\alpha)$ and $K_{II}^{l,HM}(\alpha)$ are Mode I and Mode II stress intensity factors of the isolated wing crack (l), $K_I^{2a,HM}(\alpha)$ and $K_{II}^{2a,HM}(\alpha)$ are additional Mode I and Mode II stress intensity

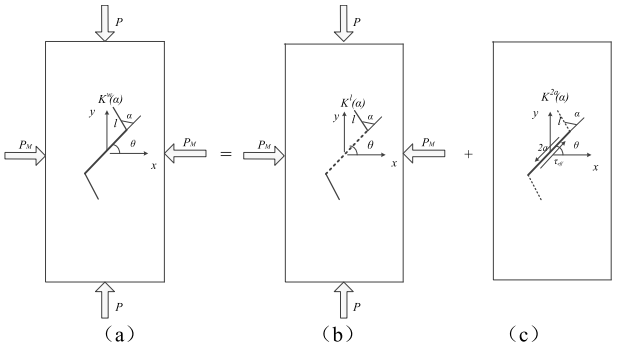

FIGURE 4. Superposition of Mode I and Mode II stress intensity factors of the isolated wing crack.

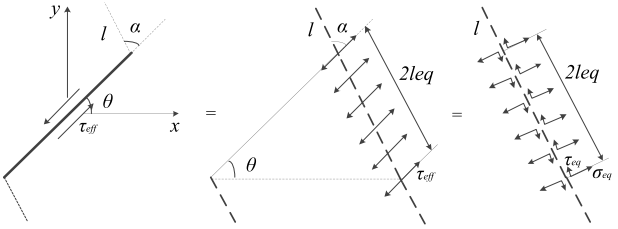

FIGURE 5. Effect of the original crack on the wing crack ($\alpha > 0$).

factors of the isolated wing crack (l) caused by the original crack ($2a$).

According to Eq. (1), there are:

$$\begin{aligned} K_I^{l,HM}(\alpha) &= \sigma_n\sqrt{\frac{\pi l}{2}} \\ &= [\frac{(P+P_M)}{2}+\frac{(P-P_M)}{2}\cos 2(\theta+\alpha)+P_H]\sqrt{\frac{\pi l}{2}} \\ K_{II}^{l,HM}(\alpha) &= \tau_n\sqrt{\frac{\pi l}{2}} \\ &= [\frac{(P-P_M)}{2}\sin 2(\theta+\alpha)]\sqrt{\frac{\pi l}{2}} \end{aligned} \tag{14}$$

For calculating $K_I^{2a,HM}(\alpha)$ and $K_{II}^{2a,HM}(\alpha)$, the effect of the original crack (length and stress) on the wing crack must be considered. On the one hand, the original crack needs to be converted into the equivalent crack length ($2l_{eq}$) in the wing crack direction. i.e., the wing crack is lengthened (Fig.5):

$$l_{eq} = \frac{a\sin\theta}{\sin(\theta+\alpha)} \tag{15}$$

On the other hand, the effective shear stress (τ_{eff}) needs be adopted and parallel transformed to the equivalent crack length, since the normal stress (σ_n) applied on the original crack plane is compressive under THM loading conditions and would results in closure of the original crack and friction force. Thus, the equivalent normal stress σ_{eq} and shear stress τ_{eq} on the equivalent crack ($2l + 2l_{eq}$) become:

$$\begin{aligned} \sigma_{eq} &= -\tau_{eff}\sin\alpha \\ \tau_{eq} &= \tau_{eff}\cos\alpha \end{aligned} \tag{16}$$

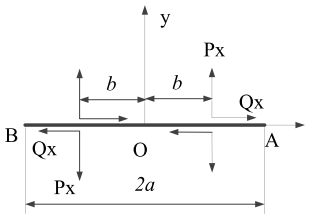

FIGURE 6. A crack under symmetrical concentrated normal and shear force.

where τ_{eff} must be negative ($P < P_M < 0$) for making the original crack slide [57], which results in tensile stress on the wing crack plane ($\sigma_{eq} > 0$). Thus, the negative sign is needed in Eq. (16).

According to the stress intensity factor formulae of a crack under symmetrical concentrated normal (P_x) and shear (Q_x) force [59] (Fig. 6,)

$$\begin{aligned} K_I &= \frac{2P}{\sqrt{\pi}}\frac{\sqrt{a}}{\sqrt{a^2-b^2}} \\ K_{II} &= \frac{2Q}{\sqrt{\pi}}\frac{\sqrt{a}}{\sqrt{a^2-b^2}} \end{aligned} \tag{17}$$

$K_I^{2a,HM}(\alpha)$ and $K_{II}^{2a,HM}(\alpha)$ can be obtained by integrating P_x and P_y in the range of l_{eq}.

$$\begin{aligned} K_I^{2a,HM}(\alpha) &= 2\sigma_{eq}\sqrt{\frac{l+l_{eq}}{\pi}}\sin^{-1}(\frac{l_{eq}}{l+l_{eq}}) \\ K_{II}^{2a,HM}(\alpha) &= 2\tau_{eq}\sqrt{\frac{l+l_{eq}}{\pi}}\sin^{-1}(\frac{l_{eq}}{l+l_{eq}}) \end{aligned} \tag{18}$$

Substituting Eqs. (15) and (16) into Eq. (18) yields

$$\begin{aligned} K_I^{2a,HM}(\alpha) &= -2\tau_{eff}\sin\alpha\sqrt{\frac{l+a\sin\theta/\sin(\theta+\alpha)}{\pi}} \\ &\quad\times\sin^{-1}\frac{a\sin\theta/\sin(\theta+\alpha)}{l+a\sin\theta/\sin(\theta+\alpha)} \\ K_{II}^{2a,HM}(\alpha) &= 2\tau_{eff}\cos\alpha\sqrt{\frac{l+a\sin\theta/\sin(\theta+\alpha)}{\pi}} \\ &\quad\times\sin^{-1}\frac{a\sin\theta/\sin(\theta+\alpha)}{l+a\sin\theta/\sin(\theta+\alpha)} \end{aligned} \tag{19}$$

Therefore, the calculation formulae of the Mode I and Mode II stress intensity factors of the wing crack ($\alpha > 0$) can be obtained by substituting Eqs. (14) and (19) into Eq. (13).

$$\begin{aligned} K_I^{w,HM}(\alpha) &= [\frac{(P+P_M)}{2}+\frac{(P-P_M)}{2}\cos 2(\theta+\alpha)+P_H]\sqrt{\frac{\pi l}{2}} \\ &\quad-2\tau_{eff}\sin\alpha\sqrt{\frac{l+a\sin\theta/\sin(\theta+\alpha)}{\pi}} \\ &\quad\times\sin^{-1}\frac{a\sin\theta/\sin(\theta+\alpha)}{l+a\sin\theta/\sin(\theta+\alpha)} \\ K_{II}^{w,HM}(\alpha) &= [\frac{(P-P_M)}{2}\sin 2(\theta+\alpha)]\sqrt{\frac{\pi l}{2}} \end{aligned}$$

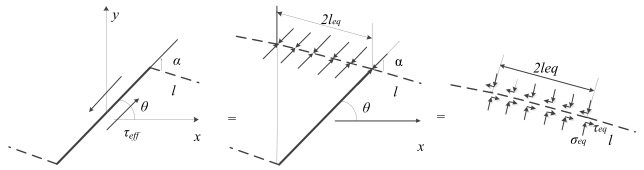

FIGURE 7. Effect of the original crack on the wing crack ($\alpha < 0$).

$$+2\tau_{eff}\cos\alpha\sqrt{\frac{l+a\sin\theta/\sin(\theta+\alpha)}{\pi}} \times \sin^{-1}\frac{a\sin\theta/\sin(\theta+\alpha)}{l+a\sin\theta/\sin(\theta+\alpha)} \quad (20)$$

2) WING CRACK INITIATED BY SHEAR ($\alpha < 0$)

Since most of pre-cracked rock specimens fail in Mode I ($\alpha > 0$), there is very few literature concerned with the case of the wing crack at $\alpha < 0$. Similar to the wing crack at $\alpha > 0$ above, Mode I and II stress intensity factor of wing crack ($\alpha < 0$) can be also obtained by the superstition method, as shown in Fig.7, i.e.,

$$l_{eq} = \frac{a\cos\theta}{\cos(\theta+\alpha)} \quad (21)$$

$$\sigma_{eq} = -\tau_{eff}\sin\alpha$$
$$\tau_{eq} = \tau_{eff}\cos\alpha \quad (22)$$

$$K_I^{w,HM}(\alpha) = [\frac{(P+P_M)}{2}+\frac{(P-P_M)}{2}\cos 2(\theta+\alpha)+P_H]\sqrt{\frac{\pi l}{2}} - 2\tau_{eff}\sin\alpha\sqrt{\frac{l+a\cos\theta/\cos(\theta+\alpha)}{\pi}} \times \sin^{-1}\frac{a\,cos\theta/cos(\theta+\alpha)}{l+a\,cos\theta/cos(\theta+\alpha)}$$

$$K_{II}^{w,HM}(\alpha) = [\frac{(P-P_M)}{2}\sin 2(\theta+\alpha) + \mu\left|\frac{(P+P_M)}{2}+\frac{(P-P_M)}{2}\cos 2(\theta+\alpha)+P_H\right|] \times\sqrt{\frac{\pi l}{2}}+2\tau_{eff}\cos\alpha\sqrt{\frac{l+a\cos\theta/\cos(\theta+\alpha)}{\pi}} \times \sin^{-1}\frac{a\cos\theta/\cos(\theta+\alpha)}{l+a\cos\theta/\cos(\theta+\alpha)} \quad (23)$$

It is noted that since the isolated wing crack is closed for Mode II fracture, the friction and surface contact are considered in the Eq. (20).

At present, there are two methods to calculate the wing-tip stress intensity factor: superposition method and complex function method. For example, Steif [57], Chen [58] and Baud *et al.* [60] adopted the superposition method to deduce the wing-tip stress intensity factor formula for the crack initiation of Mode I; Nemat-Nasser and Horri [61] used the complex function method to derive a singular integral equation of the wing-tip stress intensity factor in term of dislocation density. For verifying the wing-tip crack stress

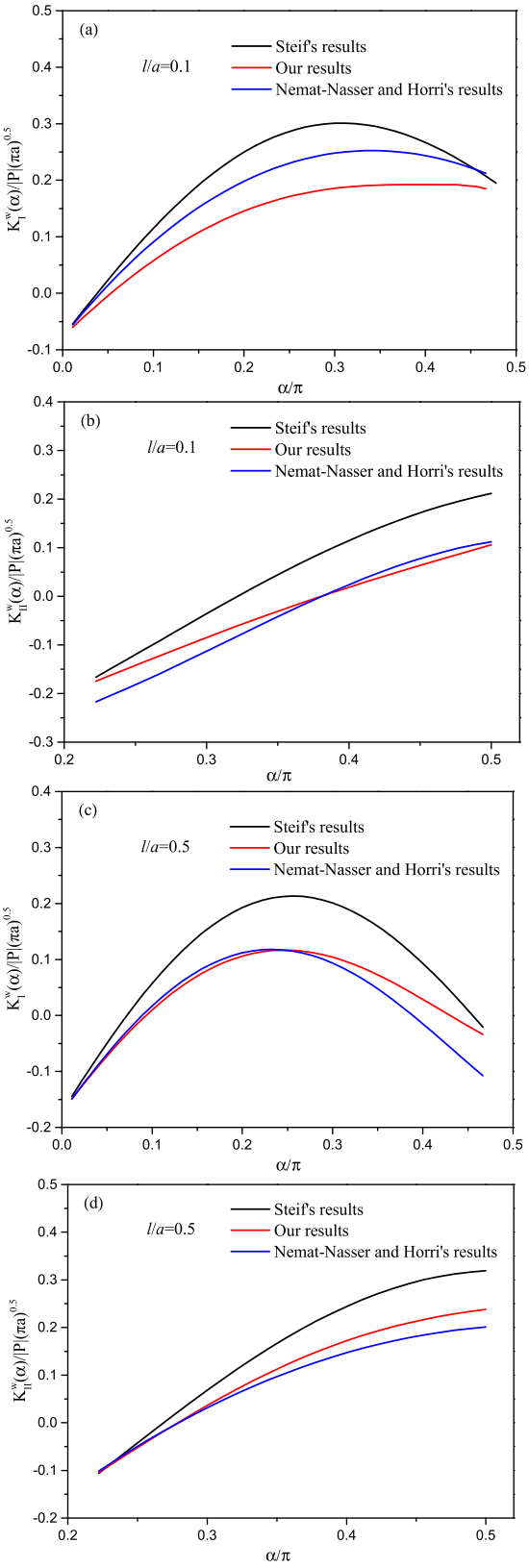

FIGURE 8. Comparison of normalized stress intensity factors of wing crack among our results, Steif's results, and Nemat-Nasser and Horri's results.

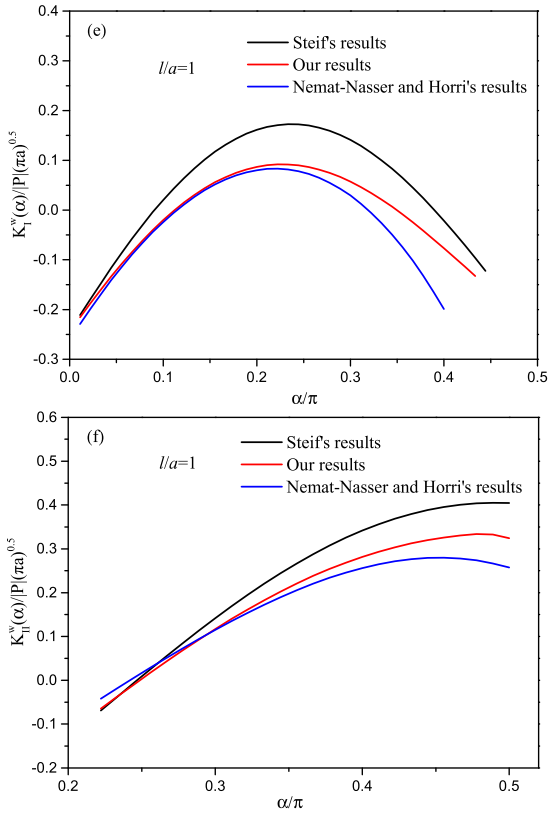

FIGURE 8. ***(Continued.)*** **Comparison of normalized stress intensity factors of wing crack among our results, Steif's results, and Nemat-Nasser and Horri's results.**

intensity factor formula of the wing crack, our calculation results of normalized stress intensity factors at wing-tips ($K_I^W = K_I^W(\alpha)/P(\pi a)^{0.5}$, $K_{II}^W = K_{II}^W(\alpha)/P(\pi a)^{0.5}$) are compared with those of Steif and Nemat-Nasser and Horri for pre-cracked specimens of same crack parameters ($\theta = 54°$, $\mu = 0.3$ and $l/a = 0.1, 0.5, 1$) under uniaxial compression ($P_H = 0$ and $P_M = 0$).

Fig. 8 shows the normalized stress intensity factors of wing crack varying with α for various crack lengths ($l/a = 0.1$, 0.5, 1). It is found that Steif's results (by the superposition method) are larger than our results and Nemat-Nasser and Horri's results (by the complex function method). Furthermore, our results are closer to Nemat-Nasser and Horri's results (exact solution) than to Steif's results, especially when l/a increases. That is because in our results, the equivalent crack length ($2l_{eq}$) is considered to calculate $K_I^{2a}(\alpha)$ and $K_{II}^{2a}(\alpha)$ caused by the original crack ($2a$), in which the total crack length is equal to $2l_{eq} + 2l$ (Fig. 5). While in Steif's results, the original crack length ($2a$) plus the wing crack length ($2l$) is simply taken to calculate $K_I^{2a}(\alpha)$ and $K_{II}^{2a}(\alpha)$. Obviously, $l_{eq} < l$ and our results are smaller and closer to Nemat-Nasser and Horri's results than Steif's results. Furthermore, for complex function method, it is difficult to obtain an explicit expression for the wing-tip stress intensity factor since the singular integral equation can only be solved numerically rather than

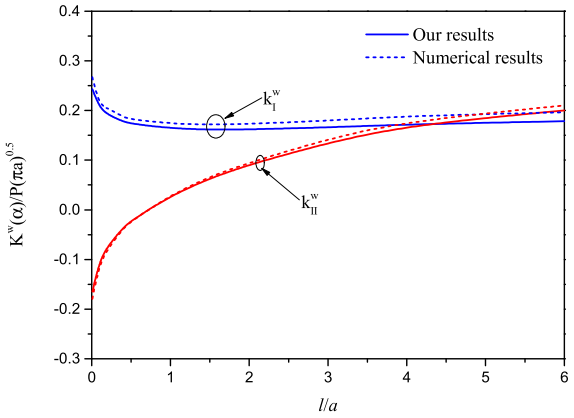

FIGURE 9. **Comparison of normalized stress intensity factors of wing crack between our results and numerical results.**

analytically. Comparatively, our method provides more precise solution than the formula of Steif and has simpler algebraic equation than the formula of Nemat-Nasser and Horri.

For further verifying the validity of the new method under complex loading conditions, ANSYS finite element method is used to calculate the stress intensity factor of wing crack, where $P = 1$MPa, $P_H = 0.1$ MPa, $P_M = 0$, $a = 15$mm, $\theta = 45°$, $\alpha = 54°$, $\mu = 0.3$. For simulating the problem by ANSYS finite element software, the length and width of the model are 200mm and 100mm, respectively, and the element type is PLANE 183. The contact element is adopted to calculate the sliding between the original crack surfaces. The stress intensity factor of wing crack can be exacted by interaction integral method after obtaining the stress and strain fields. Fig. 9 shows our results of normalized stress intensity factor at wing-tips, as well as the results of ANSYS finite element method. It is seen that with the increase of l/a, K_I^W is decreased and then increased gradually, while K_{II}^W is monotonously increased. It can be also found that in spite of small errors, our results agree very well with numerical results.

III. PREDICTION RESULTS

A. UNIAXIAL LOADING CONDITION

For prismatic rock-like material containing a single open crack ($2a = 15.2$mm) under uniaxial compression (i.e., $P_H = 0$MPa, $P_M = 0$MPa), Tables 3-4 list the predicted results of the crack initiation and unstable propagation for different inclination angles θ of the original crack, where the crack initiation load (P_C^{ini}) and angle (α_C) are calculated by the stable propagation length (l_C) and unstable propagation load (P_C^{un}) and angle (β_C) are obtained by Eqs. substituting fracture toughness ($K_{IC}^{ini} = 0.066$, $K_{IIC}^{ini} = 0.152$, $K_{IC}^{un} = 0.139$ and $K_{IIC}^{un} = 0.247$) [62] into Eq. (3) and Eq. (8-9), and (10-12). It is found that for all of θ, the crack initiation and unstable propagation have the same mechanism (i.e., Mode I fracture), since the crack initiation and the unstable propagation loads of Mode I are always smaller than those

TABLE 3. Prediction results of the crack initiation under uniaxial loading condition.

θ	Mode I		Mode II		Crack initiation		
	P_{IC}^{ini}	α_{IC}	P_{IIC}^{ini}	α_{IIC}	$P_C^{ini}=(P_{IC}^{ini}, P_{IIC}^{ini})_{\min}$	α_C	Mechanism
(°)	(MPa)	(°)	(MPa)	(°)	(MPa)	(°)	
30	1.99	102.1	2.15	-107.1	1.99	102.1	Mode I
45	1.21	95.3	2.29	-113.1	1.21	95.3	Mode I
60	1.15	82.5	3.01	-117.4	1.15	82.5	Mode I

TABLE 4. Prediction results of the crack unstable propagation under uniaxial loading condition.

θ	Mode I			Mode II			Stable propagation	Crack unstable propagation		
	l_{IC}	P_{IC}^{un}	β_{IC}	l_{IIC}	P_{IIC}^{un}	β_{IIC}	l_C	P_C^{un}	β_C	Mechanism
(°)	(mm)	(MPa)	(°)	(mm)	(MPa)	(°)	(mm)	(MPa)	(°)	
30	9.3	2.41	-80.5	9.9	3.61	-9.8	9.3	2.41	-80.5	Mode I
45	13.1	2.31	-83.2	29.6	2.58	-15.6	13.1	2.31	-83.2	Mode I
60	13.7	2.75	-87.5	11.1	3.09	-17.1	13.7	2.75	-87.5	Mode I

of Mode II. With the increase of θ, the crack initiation and unstable propagation angles are decreased while the stable propagation length becomes larger.

B. THM LOADING CONDITIONS

For the red sandstone specimens under different THM loading conditions (Fig.1), Tables 5-6 list the predicted results of the crack initiation and unstable propagation for the close crack, where the crack initiation load (P_C^{ini}) and angle (α_C) are calculated by substituting THM loading parameters (Table 1) and material parameters (Table 2) into Eq. (3) and Eq. (8-9), and the stable propagation length (l_C) and unstable propagation load (P_C^{un}) and angle (β_C) are obtained by Eqs. (10-12). It can be seen that the crack initiation and unstable propagation have the same mechanism under different THM loading conditions, i.e., when the temperature and hydraulic pressure are increased, the crack initiation and unstable propagation are gradually changed from Mode II to Mode I, while the effect of the confining pressure is opposite. That is because the high temperature and hydraulic pressure (applied onto the original crack surface) or the high confining pressure would promote or restrain the Mode I stress intensity factor. In addition, when the crack initiation and unstable propagation load of Mode I (P_{IC}^{ini}, P_{IC}^{un}) are very close to those of Mode II (P_{IIC}^{ini} and P_{IIC}^{un}), the crack initiation and unstable propagation occur in mixed mode (T3, H2, M2). It is also found that P_{IC}^{ini} and P_{IC}^{un} are smaller than P_{IIC}^{ini} and P_{IIC}^{un}, respectively, while l_{IC} is larger than l_{IIC}.

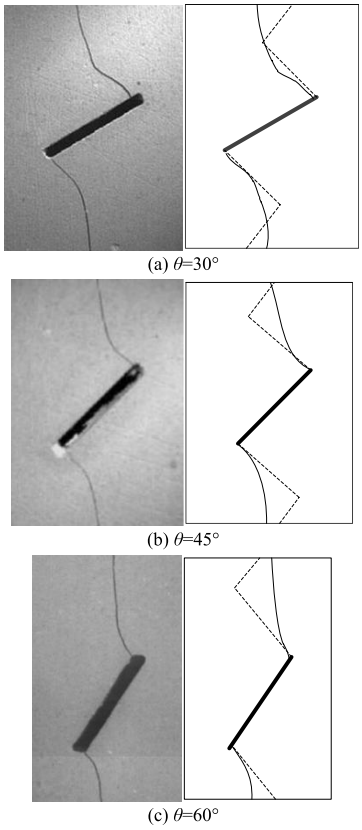
(a) θ=30°

(b) θ=45°

(c) θ=60°

FIGURE 10. Fracture trajectories of pre-cracked gypsum specimens under uniaxial compression condition.

IV. TEST VERIFICATION

A. UNIAXIAL LOADING CONDITION

Currently, many available literatures are related to the experimental investigations of the fracture trajectory of brittle material containing a single open crack. Wong *et al.* [8] investigated the crack initiation, propagation and coalescence on prismatic specimens (152mm × 76mm × 32mm) of artificially molded gypsum with an oriented open crack ($2a$ = 15.2mm) subjected to uniaxial compression. Fig. 10 demonstrates the fracture trajectory of the pre-cracked gypsum specimen for different inclination angles of the original crack. For visually comparing the predicted results with tested results, our predicted results of fracture trajectory are also depicted in Fig. 10, where the solid and dotted lines represent the tested and predicted results, respectively.

It is found that there only exists one fracture trajectory, i.e., the original crack is initiated simultaneously at the two crack tips in a positive direction ($\alpha_C > 0$), then propagated for a short length (l_C) and finally unstably propagated in a

TABLE 5. Prediction results of the crack initiation under different THM loading conditions.

No.	Mode I		Mode II		Crack initiation		Mechanism
	P_{IC}^{ini} (MPa)	α_{IC} (°)	P_{IIC}^{ini} (MPa)	α_{IIC} (°)	$P_C^{ini}=(P_{IC}^{ini}, P_{IIC}^{ini})_{\min}$ (MPa)	α_C (°)	
T1	23.2	106	21.1	-105.3	21.1	-105.3	Mode II
T2	22.9	106.7	20.3	-104.8	20.3	-104.8	Mode II
T3	20.2	107.6	20	-104.7	20.0	107.6/-104.7	Mixed mode
T4	18.5	108.1	19.5	-104.6	18.5	108.1	Mode I
H1	21.5	109.3	19.8	-103.2	19.8	-103.2	Mode II
H2	19.6	105.6	20.1	-105.7	19.6	105.6/-105.7	Mixed mode
H3	16.5	100.8	20.5	-108.4	16.5	100.8	Mode I
M1	16.6	100.6	19.4	-108.2	16.6	100.6	Mode I
M2	18.9	102.8	19.6	-107.2	18.9	102.8/-107.2	Mixed mode
M3	23.6	108.2	20.7	-103.7	20.7	-103.7	Mode II

TABLE 6. Prediction results of the crack unstable propagation under different THM loading conditions.

NO.	Mode I			Mode II			Stable propagation	Crack unstable propagation		
	l_{IC} (mm)	P_{IC}^{un} (MPa)	β_{IC} (°)	l_{IIC} (mm)	P_{IIC}^{un} (MPa)	β_{IIC} (°)	l_C (mm)	P_C^{un} (MPa)	β_C (°)	Mechanism
T1	16.9	32.5	-88.1	13.6	29.7	-18.1	13.6	29.7	-18.1	Mode II
T2	17.8	31.4	-87.9	13.9	28.8	-19.1	13.9	28.8	-19.1	Mode II
T3	14.5/16.4	25.4/29.3	-86.8/-86.2	15.6/13.4	29.2/27.8	-17.9/-18.9	15.6/13.4	29.2/27.8	-17.9/-18.9	Mixed mode
T4	18.5	22.4	-87.8	21.3	25.2	-20.1	18.5	22.4	-87.8	Mode I
H1	17.2	28.6	-88.9	13.1	27.9	-19.1	13.1	27.9	-19.1	Mode II
H2	16.2/17.1	23.5/25.2	-86.6/-87.2	18.6/13.5	27.9/24.7	-17.6/-16.5	18.6/13.5	27.9/24.7	-17.6/-16.5	Mixed mode
H3	23.2	19.8	-84.7	25.1	23.6	-16.2	23.2	19.8	-84.7	Mode I
M1	19.4	20.3	-83.2	20.1	24.4	-15.3	19.4	20.3	-83.2	Mode I
M2	16/16.2	22.7/24.9	-83.7/-85.8	17.9/13.4	27.7/24.9	-15.4/-17.2	17.9/13.4	27.7/24.9	-15.4/-17.2	Mixed mode
M3	16.3	30.8	-86.3	14.1	29.1	-19.5	14.1	29.1	-19.5	Mode II

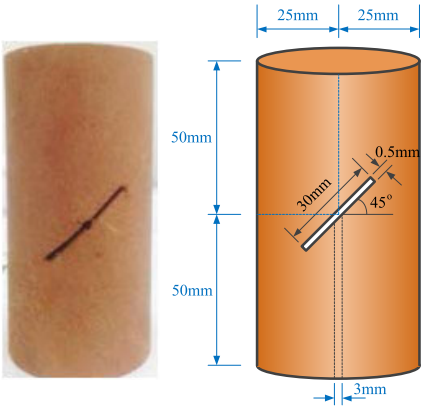

FIGURE 11. Pre-cracked red sandstone specimen.

positive direction ($\beta_C > 0$), which corresponds to typical Mode I fracture. It is also found that our results agree well with the tested results, which prove the validity of the newly established fracture theory under simple loading condition.

B. THM COUPLED FRACTURE TEST

1) TEST SCHEME

Red sandstone used in this test comes from Hunan province in China, with a good homogeneity. The main mineral composition is as follows: quartz (90.0%), hydromica (4.8%), plagioclase (2.8%), K-feldspar (1.3%) and kaolinite (1.1%) and etc. Table 7 lists the main mechanical parameters of the rock, including the tensile strength, uniaxial compressive strength, Young's modulus, friction coefficient, cohesion and internal friction angle. The cylindrical specimens of Φ50mm × 100mm are manufactured by a cutting machine with the secondary grinding by a grindstone machine for improving the machining precise (verticality and flatness). The center cracks (30mm in length and 1 mm in width) are prepared by an ultrathin diamond blade of 0.5mm in thickness. An additional vertical hole (Φ2mm × 50mm) is drilled from the bottom center of the specimen to the crack surface in order to apply the hydraulic pressure (P_H) onto the crack surface (Fig. 11).

Fig. 12 shows a self-designed THM loading system, including the tri-axial loading testing machine with a triaxial chamber, a hydraulic pressure cell (P_H by water) and a confining pressure cell (P_M by oil). In each coupled fracture test, the multi-layer polymeric abrasive paper is embedded into the crack surface for offering friction, and the temperature, hydraulic and confining pressure are unchanged. Temperature is well-controlled by heating the specimen, water and oil into the same specific value. The hydraulic and confining pressure are well-controlled by hydraulic and confining loading system, respectively. The THM loading conditions are the same as those in the above calculation model (Table 1), where $T < 100$°C for preventing water from evaporation,

(a) Tri-axial loading testing machine

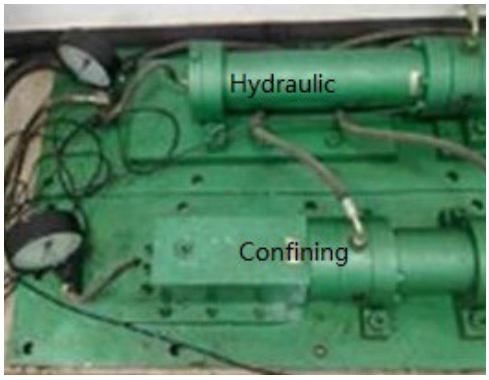

(b) Hydraulic and confining loading systems

FIGURE 12. THM loading system.

TABLE 7. Main mechanical parameters of the red sandstone.

σ_t (MPa)	σ_c (MPa)	E (GPa)	μ	c (MPa)	φ (°)
2.24	64	10.67	0.3	14	35

and $P_H < P_M$ for avoiding mixture of water and oil by wrapping the specimen with a layer of isolation films. Under the THM loading conditions, the stress-strain curve of the red sandstone specimen was registered during the test, and its fracture trajectory was examined after the test.

2) RESULTS AND ANALYSIS

As an example, Fig.13 shows the stress-strain curve of specimen T1 under THM loading conditions. It is divided into three stages: micro-pore compaction (OA, where the slope is gradually increased), elastic deformation (AB, where the slope is approximately constant), and non-elastic deformation (BC, where the slope is decreased to zero). Obviously, the crack initiation load P_C^{ini} and unstable propagation load P_C^{un} can be determined by distinguished point (B) where the curve deviates from the straight line and the peak point (C), respectively.

Fig. 14 shows fracture trajectories of the red sandstone specimens under different THM loading conditions, where the solid and dotted lines represent the tested and predicted results, respectively. The crack initiation load (P_C^{ini}) and

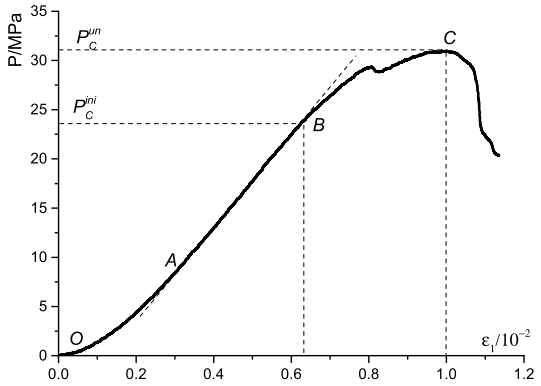

FIGURE 13. Stress-strain curve of specimen T1 under THM loading conditions.

angle (α_C), stable propagation length (l_C), and unstable propagation load (P_C^{un}) and angle (β_C) can be measured in the figure (Table 8). It is found that there exist three different fracture trajectories: (1) the original crack is first initiated simultaneously at the two tips in a positive direction ($\alpha_C > 0$), then extended for a short length (l_C) and finally unstably propagated in a positive direction ($\beta_C > 0$), which corresponds to typical Mode I fracture (T4, H3, M1); (2) the original crack is first initiated simultaneously at the two tips in a negative direction ($\alpha_C < 0$), then extended for a short length (l_C) and finally unstably propagated in a negative direction ($\beta_C < 0$), which corresponds to typical Mode II fracture (T1, T2, H1, M3); (3) when the original crack is first initiated at the two tips in two directions ($\alpha_C > 0$ and $\alpha_C < 0$), then extended for two short lengths (l_C) and finally unstably propagated in two directions ($\beta_C > 0$ and $\beta_C < 0$), which is a typical mixed mode (T3, H2, M2). Furthermore, when the temperature and hydraulic pressure are increased, the crack initiation and unstable propagation are gradually changed from Mode II to Mode I, while effect of the confining pressure is opposite. In addition, the crack initiation load (P_C^{ini}) and unstable propagation load (P_C^{un}) of Mode I are smaller than those of Mode II, while the crack stable propagation length (l_C) of Mode I is larger than that of Mode II. That is because for the brittle rock material, the crack initiation and unstable fracture toughness of Mode I ($K_{IC}^{ini,T}$ and $K_{IC}^{un,T}$) are smaller than those of Mode II ($K_{IIC}^{ini,T}$ and $K_{IIC}^{un,T}$).

Comparison of Table 8 with Tables 5-6 indicates that the test results of the crack initiation parameters, stable propagation length and unstable propagation parameters are all in good agreement with the prediction results, which proves the validity of the newly established THM coupling fracture theory.

It needs to be noted that the cylindrical samples were adopted in this test for easily applying the higher hydraulic pressure onto the original crack surface. Currently, theoretical expression of crack-tip stresses under THM loading conditions is not available for pre-cracked cylindrical sample and thus it is very difficult to deduce a calculation formula of the 3D stress intensity factor [59]. 2D theoretical

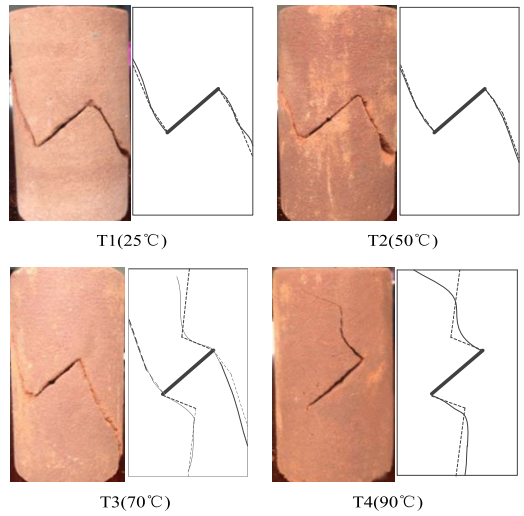

(a) At different temperatures (P_H=2MPa, P_M=4MPa)

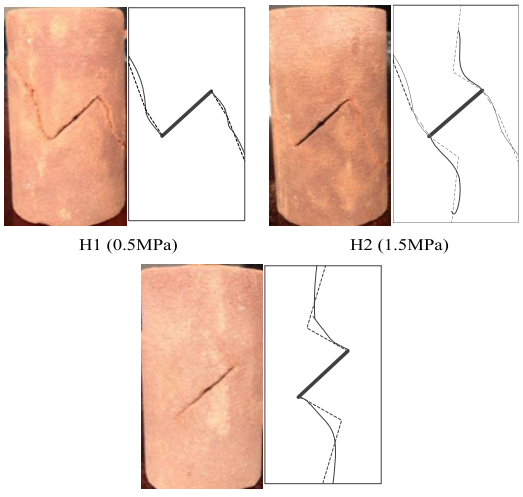

(b) At different hydraulic pressures (T=70℃, P_M=4MPa)

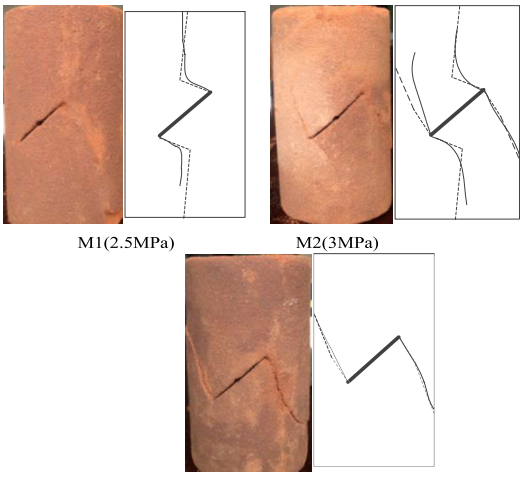

(c) At different confining pressures(T=50℃, P_H=2MPa)

FIGURE 14. Fracture trajectories of the pre-cracked red sandstone specimens under different THM loading conditions.

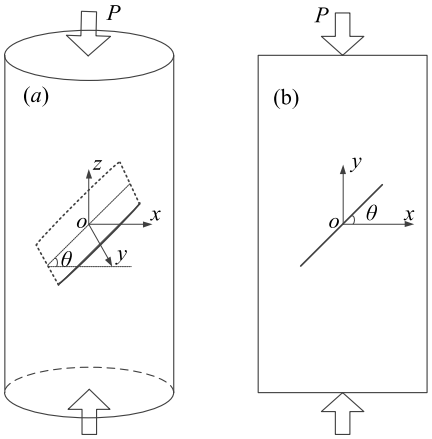

FIGURE 15. Pre-cracked cylinder model and pre-cracked plate model under uni-axial compression.

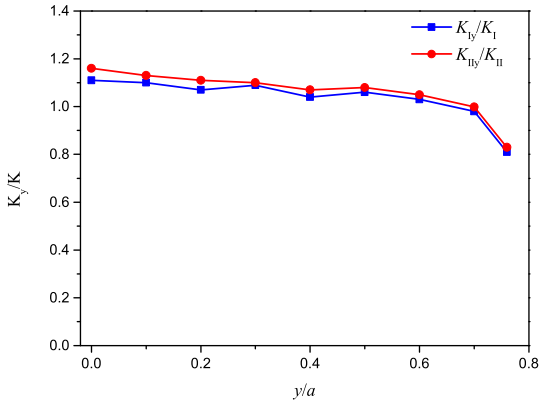

FIGURE 16. Ratio between the 3D and the 2D stress intensity factors.

model under THM loading conditions was established in this study and verified by 3D laboratory tests. Whether there is disagreement between them or not should be discussed by comparing the stress intensity factors in pre-cracked cylinder with that in pre-cracked plate.

Fig. 15 illustrates a cylinder (Φ50mm × 100mm) with a center penetrated crack (length 30mm) (Fig.15a) and a rectangular plate (50mm × 100mm) with a center crack (length 30mm) under uniaxial compression P (Fig.15b). Set a spatial coordinate system $oxyz$ at the cylinder center o. Finite element software ANSYS was used to calculate the SIFs of crack tip or front of the two models. PLANE186 (total element number is 22190) and PLANE183 (total element number is 21373) were selected in the cylinder model and in the plate mode, respectively. Elastic constitutive mode of material was applied, where E and v. The unit uniform compressive stress is applied to the specimen and the interaction integral method is adopted to determine SIFs based on the calculated the stresses and strains around the crack tip. Fig. 16 shows the ratio (K_{Iy}/K_I and K_{IIy}/K_{II}) between the 3D and the 2D stress intensity factors, where K_{Iy} and K_{IIy} are Mode I and Mode II

TABLE 8. Test results of the crack initiation, stable propagation and unstable propagation under different THM loading conditions.

NO.	Crack initiation			Stable propagation	Crack unstable propagation		
	P_C^{ini} (MPa)	α_C (°)	Mechanism	l_C (mm)	P_C^{un} (MPa)	β_C (°)	Mechanism
T1	23.2	-106.1	Mode II	15.1	30.9	-14.1	Mode II
T2	21.1	-105.4	Mode II	15.3	27.8	-20.2	Mode II
T3	19.2	109.4/-105	Mixed mode	14.7/13.2	26	-69.6/-16.6	Mixed mode
T4	17.8	98.7	Mode I	19.8	24.5	-74.3	Mode I
H1	19.4	-103.8	Mode II	15.6	26.3	-13.7	Mode II
H2	17.5	102.4/-104.7	Mixed mode	15.7/16.8	22.1	-63.9/-18.5	Mixed mode
H3	16.4	89.5	Mode I	21.1	19.1	-62.1	Mode I
M1	15.2	88.9	Mode I	17.4	18.7	-77.9	Mode I
M2	17.6	97.7/-106.8	Mixed mode	12.5/19.3	23.8	-60.1/-16.5	Mixed mode
M3	23.1	-108.4	Mode II	15.2	29.6	-13.9	Mode II

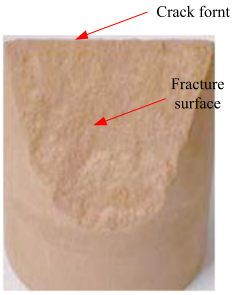

FIGURE 17. Fracture surface of pre-cracked red sandstone specimen T1.

stress intensity factors along the crack front in y direction of cylinder model, and K_{I} and K_{II} are Mode I and Mode II SIFs at crack tips in the plate model. It can be seen that from Fig. 16, both Mode I and Mode II SIFs have the maximum values at the mid-point (i.e., y = 0) of crack front similarly to the previous study [63-65]. This manifests that the real critical location of crack initiation failure is its mid-point of crack front. However, in our prediction results, the SIFs at crack front of cylindrical sample is regarded to be equal to those at crack tip of plate, i.e., $K_{\mathrm{Iy}}/K_{\mathrm{I}} = K_{\mathrm{IIy}}/K_{\mathrm{II}} = 1$. In other words, the predicted critical location of crack initiation failure is at the point y = 0.85a of crack front. Fig. 17 shows the fracture surface of the pre-cracked red sandstone specimen T1. It is observed that the fracture surface near crack front is almost flat, which suggests that crack initiation direction is the same for the entire crack front. It can be also observed that the curves of $K_{\mathrm{Iy}}/K_{\mathrm{I}}$-y/a and $K_{\mathrm{IIy}}/K_{\mathrm{II}}$-y/a are almost overlapped. Although $K_{\mathrm{Iy}}/K_{\mathrm{I}}$ and $K_{\mathrm{IIy}}/K_{\mathrm{II}}$ are decreased gradually as y/a is changed, $K_{\mathrm{Iy}}/K_{\mathrm{I}}$ and $K_{\mathrm{IIy}}/K_{\mathrm{II}}$ are approximately equal to 1. It indicates that K_{Iy} and K_{IIy} along crack front in 3D cylinder model are close to those in 2D plate model, respectively. Therefore, it should be concluded that 2D theoretical model can be applied to study 3D pre-cracked cylinder problem. In addition,

In addition, comparison of uniaxial compression tests between the pre-cracked cubic specimen [66] and the pre-cracked cylindrical specimen [67] shows that their crack propagation trajectories are almost the same, also indicating that the crack propagation pattern is little influenced by the specimen shape.

V. CONCLUSION

(1) A new THM coupling fracture theory for brittle rock is established based on a new fracture criterion of maximum tensile and shear stress intensity factor ratio. It can predict not only the crack initiation load and angle of Mode I (tension) or Mode II (shear) fracture, but also the stable propagation length and the unstable propagation load and angle of Mode I or Mode II fracture. It can be also extended to predict the crack propagation process of multi-crack problem under THM loading conditions.

(2) A new superposition method is presented to obtain Mode I and Mode II wing-tip stress intensity factors. The effectiveness of the method is verified by the conventional superposition method and the complex function method. It has not only higher accuracy than the conventional superposition method (regardless of crack effective length), but also a simpler formulation than the complex function method (singular integral equation).

(3) The crack initiation has the same mechanism as the unstable crack propagation under both uniaxial compression and THM coupling tests. When the temperature and hydraulic pressure (applied onto the original crack surface) are increased, the mechanisms of crack initiation and unstable propagation are gradually changed from Mode II to Mode I, while the effect of the confining pressure is opposite.

(4) Mode I fracture has smaller loads of crack initiation load and unstable propagation and larger length of crack stable propagation than Mode II fracture. Mode I fracture is easy to occur in brittle rock and can be easily restrained by increasing the confining pressure or decreasing the temperature and hydraulic pressure.

(5) Test results of crack initiation parameters, stable propagation length and unstable propagation parameters are all in good agreement with prediction results, which proves the validity of the new THM coupling fracture theory for brittle rock.

REFERENCES

[1] J. A. Hudson, O. Stephansson, J. Andersson, C.-F. Tsang, and L. Jing, "Coupled T–H–M issues relating to radioactive waste repository design and performance," *Int. J. Rock Mech. Mining Sci.*, vol. 38, no. 1, pp. 143–161, Jan. 2001.

[2] J. Rutqvist, M. Chijimatsu, L. Jing, A. Millard, T. S. Nguyen, A. Rejeb, Y. Sugita, and C. F. Tsang, "A numerical study of THM effects on the near-field safety of a hypothetical nuclear waste repository—BMT1 of the DECOVALEX III project. Part 3: Effects of THM coupling in sparsely fractured rocks," *Int. J. Rock Mech. Mining Sci.*, vol. 42, nos. 5–6, pp. 745–755, Jul. 2005.

[3] G. Armand, F. Bumbieler, N. Conil, R. de la Vaissière, J.-M. Bosgiraud, and M.-N. Vu, "Main outcomes from *in situ* thermo-hydro-mechanical experiments programme to demonstrate feasibility of radioactive high-level waste disposal in the callovo-oxfordian claystone," *J. Rock Mech. Geotech. Eng.*, vol. 9, no. 3, pp. 415–427, Jun. 2017.

[4] J. Zhang, H. Deng, J. Deng, and R. Gao, "Fractal analysis of pore structure development of sandstone: A nuclear magnetic resonance investigation," *IEEE Access*, vol. 7, pp. 47282–47293, 2019.

[5] A. R. Khoei, S. Moallemi, and E. Haghighat, "Thermo-hydro-mechanical modeling of impermeable discontinuity in saturated porous media with X-FEM technique," *Eng. Fract. Mech.*, vol. 96, pp. 701–723, Dec. 2012.

[6] S. Ma, Z. Luo, H. Wu, and Y. Qin, "Mechanical properties of rock with intersection structures and its progressive failure mechanism," *IEEE Access*, vol. 7, pp. 60920–60930, 2019.

[7] X. Xi, X. Wu, Q. Guo, and M. Cai, "Experimental investigation and numerical simulation on the crack initiation and propagation of rock with pre-existing cracks," *IEEE Access*, vol. 8, pp. 129636–129644, 2020.

[8] L. N. Y. Wong and H. H. Einstein, "Fracturing behavior of prismatic specimens containing single flaws," in *Proc. 41st US Symp. Rock Mech., Golden Rocks*, 2006, pp. 1–10.

[9] L. N. Y. Wong and H. H. Einstein, "Crack coalescence in molded gypsum and Carrara marble: Part 2—Microscopic observations and interpretation," *Rock. Mech. Rock. Eng.*, vol. 42, no. 3, pp. 513–545, 2008.

[10] X. Yang, Z. Qiu, and Y. Wang, "Stress interaction and crack propagation behavior of glass ceramics under multi-scratches," *J. Non-Crystalline Solids*, vol. 523, Nov. 2019, Art. no. 119600.

[11] H. Lee and S. Jeon, "An experimental and numerical study of fracture coalescence in pre-cracked specimens under uniaxial compression," *Int. J. Solids Struct.*, vol. 48, no. 6, pp. 979–999, Mar. 2011.

[12] S. Q. Yang, D. S. Yang, H. W. Jing, Y. H. Li, and S. Y. Wang, "An experimental study of the fracture coalescence behaviour of brittle sandstone specimens containing three fissures," *Rock. Mech. Rock. Eng.*, vol. 45, no. 4, pp. 563–582, 2012.

[13] S.-Q. Yang and Y.-H. Huang, "An experimental study on deformation and failure mechanical behavior of granite containing a single fissure under different confining pressures," *Environ. Earth Sci.*, vol. 76, no. 10, pp. 1–22, May 2017.

[14] Y. Niu, X. P. Zhou, J. Z. Zhang, and Q. H. Qian, "Experimental study on crack coalescence behavior of double unparallel fissure-contained sandstone specimens subjected to freeze-thaw cycles under uniaxial compression," *Cold Regions Sci. Technol.*, vol. 158, pp. 166–181, Feb. 2019.

[15] Z. Liu, C. Zhang, C. Zhang, Y. Gao, H. Zhou, and Z. Chang, "Deformation and failure characteristics and fracture evolution of cryptocrystalline basalt," *J. Rock Mech. Geotech. Eng.*, vol. 11, no. 5, pp. 990–1003, Oct. 2019.

[16] Y.-H. Huang, S.-Q. Yang, W.-L. Tian, W. Zeng, and L.-Y. Yu, "An experimental study on fracture mechanical behavior of rock-like materials containing two unparallel fissures under uniaxial compression," *Acta Mech. Sinica*, vol. 32, no. 3, pp. 442–455, Jun. 2016.

[17] S. Gali and K. V. L. Subramaniam, "Evaluation of crack propagation and post-cracking hinge-type behavior in the flexural response of steel fiber reinforced concrete," *Int. J. Concrete Struct. Mater.*, vol. 11, no. 2, pp. 365–375, Jun. 2017.

[18] K. C. Reddy and K. V. L. Subramaniam, "Experimental investigation of crack propagation and post-cracking behaviour in macrosynthetic fibre reinforced concrete," *Mag. Concrete Res.*, vol. 69, no. 9, pp. 467–478, May 2017.

[19] F. Erdogan and G. C. Sih, "On the crack extension in plates under plane loading and transverse shear," *J. Basic Eng.*, vol. 85, no. 4, pp. 519–527, 1963.

[20] S. K. Maiti and R. A. Smith, "Comparison of the criteria for mixed mode brittle fracture based on the preinstability of stress-strain field," *Int. J. Fract.*, vol. 24, no. 2, pp. 5–22, 1984.

[21] M.-H. Yu, "Twin shear stress yield criterion," *Int. J. Mech. Sci.*, vol. 25, no. 1, pp. 71–74, Jan. 1983.

[22] K. J. Chang, "On the maximum strain criterion—A new approach to the angled crack problem," *Eng. Fract. Mech.*, vol. 14, no. 1, pp. 107–124, Jan. 1981.

[23] G. C. Sih, "Strain-energy-density factor applied to mixed mode crack problems," *Int. J. Fract.*, vol. 10, no. 3, pp. 305–321, 1974.

[24] K. Palaniswamy and W. G. Knauss, "Propagation of a crack under general, in-plane tension," *Int. J. Fract. Mech.*, vol. 8, no. 1, pp. 114–117, Mar. 1972.

[25] M. A. Hussain, S. L. Pu, and J. Underwood, *Strain Energy Release Rate for a Crack Under Combined Mode I and Mode II*, Standard Fracture Analysis ASTM STP 560, American Society for Testing and Materials, Philadelphia, PA, USA, 1974, pp. 2–28.

[26] P. S. Theocaris and N. P. Andrianopoulos, "The mises elastic-plastic boundary as the core region in fracture criteria," *Eng. Fract. Mech.*, vol. 16, no. 3, pp. 425–432, Jan. 1982.

[27] P. S. Theocaris, G. A. Kardomateas, and N. P. Andrianopoulos, "Experimental study of the T-criterion in ductile fracture," *Eng. Fract. Mech.*, vol. 17, no. 5, pp. 439–447, 1982.

[28] P. S. Theocaris and N. P. Andrianopoulos, "The T-criterion applied to ductile fracture," *Int. J. Fract.*, vol. 20, pp. 125–130, Dec. 1982.

[29] N. A. B. Yehia, "Distortional strain energy density criterion: The Y-criterion," *Eng. Fract. Mech.*, vol. 39, no. 3, pp. 477–485, Jan. 1991.

[30] M. R. M. Aliha and M. R. Ayatollahi, "Rock fracture toughness study using cracked chevron notched Brazilian disc specimen under pure modes I and II loading—A statistical approach," *Theor. Appl. Fract. Mech.*, vol. 69, pp. 17–25, Feb. 2014.

[31] M.-D. Wei, F. Dai, N.-W. Xu, J.-F. Liu, and Y. Xu, "Experimental and numerical study on the cracked chevron notched semi-circular bend method for characterizing the mode I fracture toughness of rocks," *Rock Mech. Rock Eng.*, vol. 49, no. 5, pp. 1595–1609, May 2016.

[32] M. Talukdar, D. G. Roy, and T. N. Singh, "Correlating mode-I fracture toughness and mechanical properties of heat-treated crystalline rocks," *J. Rock Mech. Geotech. Eng.*, vol. 10, no. 1, pp. 91–101, Feb. 2018.

[33] M. R. M. Aliha, M. R. Ayatollahi, and B. Kharazi, "Mode II brittle fracture assessment using ASFPB specimen," *Int. J. Fract.*, vol. 159, no. 2, pp. 241–246, Oct. 2009.

[34] T. Backers and O. Stephansson, "ISRM suggested method for the determination of mode II fracture toughness," *Rock Mech. Rock Eng.*, vol. 45, no. 6, pp. 1011–1022, Nov. 2012.

[35] M. Sistaninia and M. Sistaninia, "Theoretical and experimental investigations on the mode II fracture toughness of brittle materials," *Int. J. Mech. Sci.*, vol. 98, pp. 1–13, Jul. 2015.

[36] M. R. Ayatollahi and M. R. M. Aliha, "Analysis of a new specimen for mixed mode fracture tests on brittle materials," *Eng. Fract. Mech.*, vol. 76, no. 11, pp. 1563–1573, Jul. 2009.

[37] Y. Li, N. Fantuzzi, and F. Tornabene, "On mixed mode crack initiation and direction in shafts: Strain energy density factor and maximum tangential stress criteria," *Eng. Fract. Mech.*, vol. 109, pp. 273–289, Sep. 2013.

[38] L. Ren, L. Z. Xie, H. P. Xie, T. Ai, and B. He, "Mixed-MODE fracture behavior and related surface topography feature of a typical sandstone," *Rock. Mech. Rock. Eng.*, vol. 49, no. 8, pp. 1–17, 2016.

[39] M. M. Mirsayar, F. Berto, M. R. M. Aliha, and P. Park, "Strain-based criteria for mixed-mode fracture of polycrystalline graphite," *Eng. Fract. Mech.*, vol. 156, pp. 114–123, May 2016.

[40] M. M. Mirsayar, A. Razmi, and F. Berto, "Tangential strain-based criteria for mixed-mode I/II fracture toughness of cement concrete," *Fatigue Fract. Eng. Mater. Struct.*, vol. 41, no. 1, pp. 129–137, Jan. 2018.

[41] S. Ghouli, M. R. Ayatollahi, and A. R. Bushroa, "Fracture characterization of ceria partially stabilized zirconia using the GMTSN criterion," *Eng. Fract. Mech.*, vol. 199, pp. 647–657, Aug. 2018.

[42] H. Karimzadeh, A. Razmi, R. Imaninasab, and A. Esminejad, "The influence of natural and synthetic fibers on mixed mode I/II fracture behavior of cement concrete materials," *Can. J. Civil Eng.*, vol. 46, no. 12, pp. 1081–1089, Dec. 2019.

[43] B. Dehghani and L. Faramarzi, "Experimental investigations of fracture toughness and crack initiation in marble under different freezing and thermal cyclic loading," *Construct. Building Mater.*, vol. 220, pp. 340–352, Sep. 2019.

[44] Q. Rao, Z. Sun, O. Stephansson, C. Li, and B. Stillborg, "Shear fracture (mode II) of brittle rock," *Int. J. Rock Mech. Mining Sci.*, vol. 40, no. 3, pp. 355–375, Apr. 2003.

[45] Q. H. Rao, *Pure Shear Fracture of Brittle Rock: A Theoretical and Laboratory Study*. Luleå, Sweden: Luleå Univ. of Technology, 1999.

[46] H. F. Xie, Q. H. Rao, and Q. Xie, "Plane shear (mode II) fracture experiment analysis of brittle rock at high temperature," (in Chinese), *Trans. Nonferrous Met. Soc.*, vol. 18, no. 8, pp. 1534–1542, 2008.

[47] M. R. Ayatollahi and M. R. M. Aliha, "Fracture toughness study for a brittle rock subjected to mixed mode I/II loading," *Int. J. Rock Mech. Mining Sci.*, vol. 44, no. 4, pp. 617–624, Jun. 2007.
[48] L. Peng, R. Qiuhua, and M. Wenbo, "Coupled thermo-hydro-mechanical fractographic analysis of brittle rock," (in Chinese), *Chin. J. Rock. Mech. Eng.*, vol. 33, no. 6, pp. 1179–1186, 2014.
[49] D. A. Chuprakov and A. S. Zhubayev, "A variational approach to analyze a natural fault with hydraulic fracture based on the strain energy density criterion," *Theor. Appl. Fract. Mech.*, vol. 53, no. 3, pp. 221–232, Jun. 2010.
[50] J. Luo and L. Wang, "High-temperature mechanical properties of mudstone in the process of underground coal gasification," *Rock Mech. Rock Eng.*, vol. 44, no. 6, pp. 749–754, Nov. 2011.
[51] A. Barua, S. Kim, Y. Horie, and M. Zhou, "Ignition criterion for heterogeneous energetic materials based on hotspot size-temperature threshold," *J. Appl. Phys.*, vol. 113, no. 6, pp. 1–22, 2013.
[52] A. Ghanbari and S. S. Rad, "Development of an empirical criterion for predicting the hydraulic fracturing in the core of Earth dams," *Acta Geotech.*, vol. 10, no. 2, pp. 243–254, Apr. 2015.
[53] F. Berto and P. Gallo, "Extension of linear elastic strain energy density approach to high temperature fatigue and a synthesis of Cu-Be alloy experimental tests," *Eng. Solid Mech.*, vol. 3, no. 2, pp. 111–116, 2015.
[54] P. Mamot, S. Weber, T. Schröder, and M. Krautblatter, "A temperature- and stress-controlled failure criterion for ice-filled permafrost rock joints," *Cryosphere*, vol. 12, no. 10, pp. 3333–3353, Oct. 2018.
[55] Y. Zhang and B. Zhang, "Mechanism of zonal disintegration in surrounding rock mass around deep rock engineering and its application," *Sci. China Technol. Sci.*, vol. 54, no. S1, pp. 221–227, Dec. 2011.
[56] W. Yi, Q.-H. Rao, S. Luo, Q.-Q. Shen, and Z. Li, "A new integral equation method for calculating interacting stress intensity factor of multiple crack-hole problem," *Theor. Appl. Fract. Mech.*, vol. 107, Jun. 2020, Art. no. 102535.
[57] P. S. Steif, "Crack extension under compressive loading," *Eng. Fract. Mech.*, vol. 20, no. 3, pp. 463–473, Jan. 1984.
[58] F. Chen, "The theoretical and experimental investigation on rock fracture due to shear-compression loading," Central South Univ., Changsha, China, Tech. Rep., 2002, pp. 17–22.
[59] T. L. Anderson, *Fracture Mechanics: Fundamentals and Applications*. Boca Raton, FL, USA: CRC Press, 1991.
[60] P. Baud, T. Reuschlé, and P. Charlez, "An improved wing crack model for the deformation and failure of rock in compression," *Int. J. Rock. Mech. Mining Sci.*, vol. 33, no. 5, pp. 539–542, 1996.
[61] S. Nemat-Nasser and H. Horii, "Compression-induced nonplanar crack extension with application to splitting, exfoliation, and rockburst," *J. Geophys. Res., Solid Earth*, vol. 87, no. B8, pp. 6805–6821, Aug. 1982.
[62] X.-P. Zhang and L. N. Y. Wong, "Cracking processes in rock-like material containing a single flaw under uniaxial compression: A numerical study based on parallel bonded-particle model approach," *Rock Mech. Rock Eng.*, pp. 711–737, Nov. 2011.
[63] M. R. M. Aliha and A. Bahmani, "Rock fracture toughness study under mixed mode I/III loading," *Rock. Mech. Rock. Eng.*, vol. 50, no. 7, pp. 1–13, 2017.
[64] A. Bahmani, M. R. M. Aliha, and F. Berto, "Investigation of fracture toughness for a polycrystalline graphite under combined tensile-tear deformation," *Theor. Appl. Fract. Mech.*, vol. 90, pp. 643–653, Aug. 2017.
[65] M. R. M. Aliha, A. Bahmani, and S. Akhondi, "Numerical analysis of a new mixed mode I/III fracture test specimen," *Eng. Fract. Mech.*, vol. 134, pp. 95–110, Jan. 2015.
[66] T. Liu, B. Lin, and W. Yang, "Mechanical behavior and failure mechanism of pre-cracked specimen under uniaxial compression," *Tectonophysics*, vols. 712–713, pp. 330–343, Aug. 2017.
[67] Y. Wang, J. Tang, Z. Dai, and T. Yi, "Experimental study on mechanical properties and failure modes of low-strength rock samples containing different fissures under uniaxial compression," *Eng. Fract. Mech.*, vol. 197, pp. 1–20, Jun. 2018.